

Holes and Entrainment in Stratocumulus

H. GERBER AND G. FRICK

Gerber Scientific Inc., Reston, Virginia

S. P. MALINOWSKI

Warsaw University, Warsaw, Poland

J.-L. BRENGUIER AND F. BURNET

Météo-France, Toulouse, France

(Manuscript received 26 November 2003, in final form 31 July 2004)

ABSTRACT

Aircraft flights through stratocumulus clouds (Sc) during the Dynamics and Chemistry of Marine Stratocumulus II (DYCOMS-II) study off the California coast found narrow in-cloud regions with less liquid water content (LWC) and cooler temperatures than average background values. The regions are named cloud holes and are assumed to be a result of water evaporated by the entrainment of dryer air from above the Sc. While such features have been noted previously, this study provided a unique opportunity to investigate in much greater detail the nature of the holes, as well as their relationship to the entrainment rate, because high-speed temperature and LWC probes with maximum spatial resolution of 10 cm were flown together for the first time. Nine long-duration flights were made through mostly unbroken Sc for which conditional sampling was used to identify the location and size of the holes. The holes are concentrated near cloud top, their average width near cloud top is about 5 m, their relative length distribution is nearly constant for all flights, and they can penetrate hundreds of meters deep into the Sc before being lost by mixing. Entrainment velocities at cloud top are estimated from measurements of fluxes of reduced LWC and vapor mixing ratios in holes, the fraction of cloud area covered by holes, and the total water jump between cloud top and the free atmosphere. Rates as large as 10 mm s^{-1} are found for nocturnal flights, and these rates are about 3 times larger than for daytime flight segments. The rates correlate best with the size of the buoyancy jump above the Sc; the present conditional-sampling approach for measuring the rates gives larger rates than the “flux jump” rates determined by others for the same flights by a factor of about 2. The stability criterion for all Sc predicts thinning and breakup of the Sc, which does not occur. The minimal amount of cloud-top evaporative cooling caused by entrainment contributes little to the top-down convection dominated by radiative cooling during nocturnal flights; however, evaporative cooling caused by the mixing of holes as they subduct with the large-scale eddy circulation in the Sc may contribute, but with an as-of-yet unknown amount.

1. Introduction

A striking feature of in situ observations made in largely unbroken stratocumulus clouds (Sc) during the Dynamics and Chemistry of Marine Stratocumulus II (DYCOMS-II; Stevens et al. 2003a) field study is the omnipresence of narrow cloud regions with sharply reduced liquid water content (LWC) in comparison to a slowly varying LWC background (see Fig. 1). We define the depleted LWC in these features as the “indicator variable” (Khalsa 1993) used in conditional data sampling to fix the location of cloud regions assumed to

be affected by the entrainment of dryer and warmer air from above the Sc. We further name the regions *cloud holes* (Korolev and Mazin 1993). The regions have also been given names including *turbules* (Rogers and Telford 1986; Telford and Keck 1988), *downdraughts* (Nicholls 1989), *plumes and convective elements* (Moeng and Schumann 1991), *wisps* (Krueger 1993), and *entrainment events* (Khalsa 1993; Wang and Albrecht 1994; Wang and Lenschow 1995).

A method described by Nicholls (1989) and also applied by Khalsa (1993) and Wang and Albrecht (1994) uses conditionally sampled cloud-hole data for calculating the entrainment velocity (w_e) into the Sc. This velocity is the average rate at which overlying drier and warmer air is entrained into the top of Sc causing LWC evaporation and potential breakup of the Sc. The

Corresponding author address: Dr. H. Gerber, Gerber Scientific Inc., 1643 Bentana Way, Reston, VA 20190.
E-mail: hgerber6@comcast.net

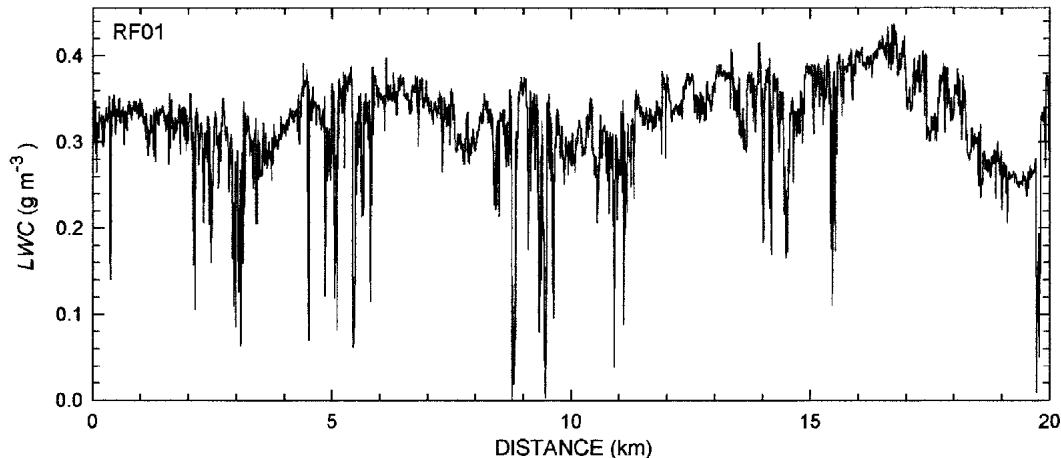


FIG. 1. LWC measured at 4-m resolution during horizontal flight of the NCAR C-130 aircraft 100 m below Sc top on flight RF01 of the DYCOMS-II study. Narrow regions of reduced LWC are interpreted as holes caused by the entrainment of air at cloud top.

cloud-hole method for estimating w_e equates the mass transport rate of water across the entraining interface with the transport rate near cloud top of depleted water in the holes. This differs from the more commonly used “flux jump” approach based on the work by Lilly (1968), where w_e is given by the flux of a scalar quantity near cloud top divided by the jump in value of the quantity between the cloud and the free atmosphere above. Recent examples of the latter approach used with DYCOMS-II data are given in Stevens et al. (2003b) and Faloon et al. (2003, manuscript submitted to *J. Atmos. Sci.*, hereafter FAL). The application of the conditional-sampling approach requires subjectivity when applying the indicator variable, which causes some uncertainty in the results, whereas, the flux-jump approach does not share this constraint. However, the former approach permits a close look at cloud holes, which may improve our incomplete understanding of the entrainment process.

This observational study has two main topics: First, we characterize Sc cloud holes using the DYCOMS-II dataset collected with probes on the National Center for Atmospheric Research (NCAR) C-130 research aircraft. The characterization is unique because this field study provided the first opportunity to fly together a set of probes with greatly improved spatial resolution for in-cloud measurements. The probes include the particle volume monitor (PVM; Gerber et al. 1994) used for LWC and effective droplet radius measurements, the ultrafast thermometer (UFT; Haman et al. 2001) used for temperature measurements, and the Fast Forward Scattering Spectrometer Probe (FFSSP; Brenguier et al. 1998) used for measurements of droplet spectra. The former two probes have the capability of resolving cloud scales as small as 10 cm, and the latter 2 m. With the enhanced resolution of these probes, it will be possible to estimate if the smaller spatial resolution used

previously to determine hole properties was sufficient to avoid errors caused by unresolved hole details. Second, we calculate mean values of w_e for the DYCOMS-II Sc by using the conditional sampling of cloud holes with an approach closely related to the one described by Nicholls (1989). Published values of w_e for Sc (e.g., see Nicholls and Leighton 1986; Kawa and Pearson 1989; Khalsa 1993; Wang and Albrecht 1994; Wang and Lenschow 1995) have shown large variability that could be caused by natural Sc variability or by measurement error. The latter has a finite probability given that the measurement of w_e has a reputation of being difficult to make. The conditional-sampling approach applied here has the advantage of utilizing data from improved instrumentation that could improve measurement accuracy. It also provides the opportunity of comparing w_e determined in this fashion with the earlier work as well as with the flux-jump approach used by FAL for calculating w_e for the same DYCOMS-II flights.

The following sections include, sequentially, descriptions of the Nicholls entrainment-rate concept, the conditional-sampling method used to identify cloud holes, the horizontal and vertical variability of depleted water in the Sc, the calculation of w_e , and the entrainment process.

2. Entrainment concept

The formulation of w_e , given measurements of the total water mixing ratio (q_T) and of the conditionally sampled cloud holes, equates the rate of total water transport through the cloud-top interface due to entrainment to the transport at cloud top of depleted water in the holes (see Fig. 2). Entrainment causes a deficit of q_T at cloud top that is described by the deficit water mass transport across the cloud-top interface

the spatial resolution of the high-data-rate LWC measurements.

The identification of holes from the LWC record uses a multicriterion method that establishes the boundaries between LWC_h in the holes and the background LWC_c . The following steps are used (see Fig. 3):

- 1) A background LWC_c level is established by using a first running average of 25-Hz LWC data (4-m resolution at the nominal aircraft speed of 100 m s^{-1}) over a flight distance, L , of several hundred meters.
- 2) The first running average is adjusted by multiplying it with a factor $K1 < 1.00$.
- 3) All LWC values of the original data with values less than the adjusted running average are deleted, forming data gaps.
- 4) The original data, including the gaps, are then given a second running average over L , and the average is multiplied by a factor $K2 < 1.00$ resulting in $LWC_c \times K2$.
- 5) The intersections of the original LWC data with $LWC_c \times K2$ are defined as the boundaries of the holes.

The method of using $K1$, $K2$, and L gives background LWC_c values with most of the influence of the holes removed, thus reducing the underestimation of background LWC_c , and preventing an undue influence from the small-amplitude fluctuation in the LWC data. The numerical choices of the criteria will obviously influence the value LWC' , but will also affect values of A_r as well as w' in the holes. The choices are made by assuming that the most appropriate values are consistent with the largest values of A_r times the LWC' flux in the

holes. Table 1 shows the results of sensitivity calculations that vary the numerical values of the criteria, $K1$, $K2$, L , and L_w ; L_w is the flight distance used to produce a running average of w , which is subtracted from the original w data to reduce offsets and trends. The results in Table 1 are based on 25-Hz data collected during a 60-km horizontal segment flown by the C-130 about 100 m below the top of mostly unbroken Sc on flight RF01. Table 1 shows that the mean value of $A_r \times LWC'$ flux is quite insensitive to the values chosen for the criteria, with small values of $K1$, L , and L_w giving the smallest values of $A_r \times LWC'$ flux, and with changes in A_r and $LWC' \times w'$ approximately inversely proportional to each other. The choice made for the criteria values and applied in the following are $L = 400 \text{ m}$, $L_w = 8 \text{ km}$, $K1 = 0.95$, and $K2 = 0.93$.

An example of the conditionally sampled LWC' flux for the 1-h horizontal flight 100 m below cloud top for flight RF01 is shown in Fig. 4, where high correlation is seen between LWC' and downdrafts (positive values), although some $LWC' \times w'$ is also found in updrafts (negative values). The density of the flux along the flight path shows significant variability, which can be a result of natural variability or the inability to determine accurately the distance flown below the undulating cloud top.

4. Cloud-top flights

The DYCOMS-II study was held in July 2001 off the southern California coast. Nine of ten flights of the NCAR C-130 aircraft found Sc located in an area about 1-h flight time west-southwest of San Diego. Most of the flights were nocturnal, beginning about 11 PM local time. The exceptions were flights RF08 and RF09, which began in the afternoon. On each flight, the aircraft spent about 6 h on-site conducting soundings, horizontal circular legs above, in, and below the clouds, and shallow profiling near cloud top [see Stevens et al. (2003a) for additional details of aircraft deployment]. The two circular legs about 30-min long and flown in opposite directions and about 100 m below cloud top, on most flights produced data suitable for estimating w_e using the present conditional-sampling approach. Table 2 lists the nine flights, dates, and time intervals for the cloud-top legs, and other basic cloud information. Cloud-top flight segments were conducted twice on flights RF08 and RF09 for the purpose of studying diurnal effects. The first segment was flown in the afternoon and the second in the evening. The evening cloud-top flight was done after sunset for RF08, and just before sunset for RF09. RF03, RF04, RF06, and RF09 had horizontal legs below cloud top less than the planned-for 60 min; consecutively, data recording was sporadic, the PVM instrument failed after 21 min, the aircraft did not fly circular legs on this flight and only flew just below cloud top on six separate short time intervals

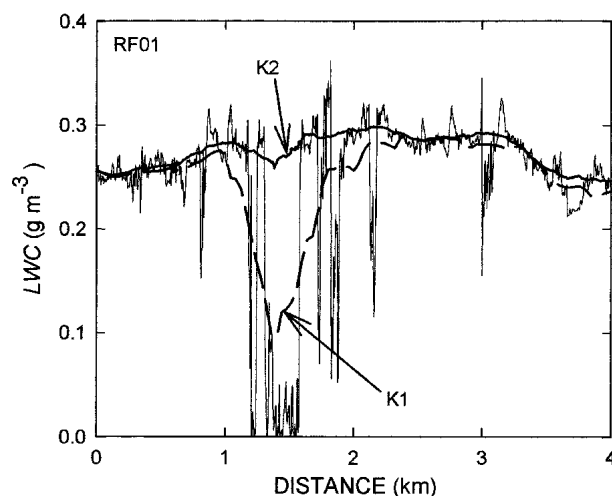


FIG. 3. Example of determining low-pass-filtered background LWC_c curves (dashed and dark lines) obtained with a two-step method that minimizes the effect of the holes on background LWC_c values. The second step produces the curve identified by $K2$, which is a constant subsequently applied to the background LWC_c curve to minimize the effect of small LWC fluctuations on the conditional sampling of the holes.

TABLE 1. Average flux $w' \times LWC'$ of depleted LWC' in cloud holes and fractional cloud area A_r as a function of the averaging flight distance L for background LWC and L_w for vertical velocity w , and of parameters K1 and K2 used for conditional identification of the holes.

L (km)	L_w (km)	K1	K2	$\langle w' \times LWC' \rangle$ ($g\ cm^{-2}\ s^{-1}$)	A_r	$A_r \langle w' \times LWC' \rangle$ ($g\ cm^{-2}\ s^{-1}$)
0.60	8.0	0.95	0.93	0.0395	0.186	0.007 34
0.80	8.0	0.95	0.90	0.0556	0.132	0.007 33
0.80	8.0	0.95	0.93	0.0365	0.200	0.007 29
0.60	8.0	0.95	0.90	0.0602	0.121	0.007 27
0.32	6.4	0.95	0.93	0.0438	0.165	0.007 25
0.40	8.0	0.95	0.93	0.0432	0.168	0.007 24
0.32	8.0	0.95	0.93	0.0440	0.164	0.007 21
0.32	6.4	0.97	0.95	0.0292	0.247	0.007 21
0.40	6.4	0.95	0.93	0.0430	0.168	0.007 21
0.80	6.4	0.95	0.90	0.0579	0.124	0.007 20
0.32	6.4	0.95	0.92	0.0504	0.142	0.007 19
0.24	6.4	0.95	0.93	0.0453	0.157	0.007 12
0.32	6.4	0.92	0.90	0.0679	0.102	0.006 94
0.32	4.0	0.95	0.93	0.0414	0.164	0.006 88
0.40	2.0	0.95	0.93	0.0376	0.168	0.006 31
0.40	0.8	0.95	0.93	0.0299	0.168	0.005 01

totaling 45 min, and opposite-direction circles were not flown. Vertical profiles of the Sc were flown occasionally during each flight. Linear regression of PVM LWC data (filtered to 1 Hz) from all the profiles is used to estimate the average for the subcloud segments of cloud-top height (z_i), cloud base (z_o), cloud thickness ($z_i - z_o$), and the distance flown below cloud top ($z_i - z_a$), where z_a is the aircraft level. The maximum LWC at the top of the Sc determined for all profiles is averaged to establish LWC_i .

a. Hole size distributions

Conditional sampling using the 25-Hz DYCOMS-II data is applied to the time intervals listed in Table 2 for determining statistics related to the length of the LWC' holes as the aircraft flew at z_a . Table 3 lists the average density N of holes per kilometer, the percentage p of flight path over which $LWC = 0$, and the fraction A_r of the flight path containing holes. The value of p evaluated with the 25-Hz data is approximately zero for the three flights with the most vigorous entrainment. However, the higher-resolution 1000-Hz LWC data show more locations with $LWC = 0$ in those Sc.

Figure 5 gives the frequency and number distribution of hole lengths for all the flights. The top panel of Fig. 5 shows that the frequency distribution of lengths is nearly the same for all flights, with the variability at large lengths caused presumably by their rarity. Duroure and Guillemet (1990) and Korolev and Mazin (1993) give frequency versus length curves of stratocumulus inhomogeneities similar to the one in the top panel. Nicholls (1989) writes, "The number of larger events (lengths) encountered in the measurements may thus be largely explained by oblique intersections of relatively narrow areas (holes)." This suggestion is also appropriate for explaining the consistency of the frequency distributions of the present Sc data when the

width perpendicular to the long dimension of the holes is assumed to be significantly smaller than the lengths of the oblique intersections. To estimate the widths of the holes it is necessary to assume the geometry of the holes. Nicholls (1989) suggested that the downdrafts took on the appearance of areas of uniform width surrounding hexagonal updraft cells, with the width of the downdrafts approximately equal to 0.1 to 0.15 h , where h is the mixed-layer depth. In our case we assume that the horizontal shapes of the holes are narrow rectangles with a maximum long dimension of 200 m. We further assume that the width of the holes is lognormally distributed and that the aircraft penetrates the holes at a random angle to give a distribution of hole lengths. The Monte Carlo approach is used to estimate the parameters of the lognormal distribution of

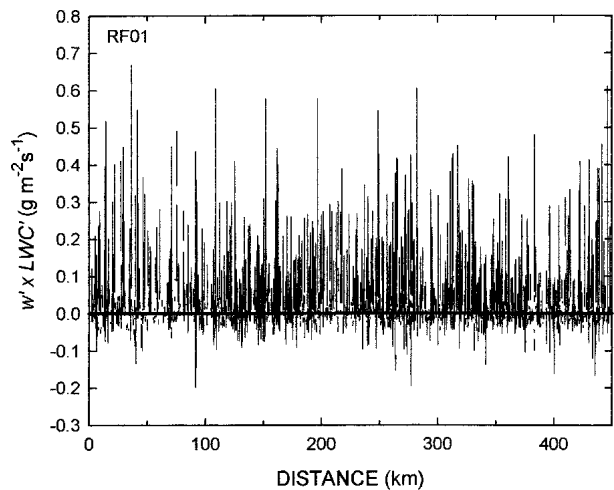


FIG. 4. The flux of depleted LWC' in the holes as a function of the 1-h horizontal flight distance of the aircraft 100 m below stratocumulus top on flight RF01.

TABLE 2. List of flights of the NCAR C-130 during the DYCOMS-II study of stratocumulus of the southern coast of California. The start indicates the beginning time (UTC) of horizontal flight legs of given duration at the aircraft level z_a about 100 m below cloud top that were evaluated in this study. The first seven flights each started near midnight local time. The height z and cloud parameters are explained in the text.

Flight	Date (Jul)	Start (UTC)	Duration (min)	z_i (m)	$z_i - z_o$ (m)	$z_i - z_a$ (m)	T_i (°C)	ΔT (°C)	P_i (mb)	LWC_i (g m ⁻³)	q_{vi} (g kg ⁻¹)	Δq_v (g kg ⁻¹)	ρ_i (kg m ⁻³)
RF01	10	1034	60	820	260	100	12.0	9.8	922	0.57	8.58	-7.38	1.13
RF02	11	1107	64	705	325	80	12.7	7.3	964	0.55	9.19	-7.52	1.17
RF03	13	1003	39	665	350	130	12.5	7.5	975	0.75	9.99	-6.20	1.19
RF04	17	1127	21	1010	505	125	11.3	6.0	903	0.87	8.61	-3.34	1.10
RF05	18	1100	65	875	245	150	9.2	6.4	917	0.58	9.64	-6.34	1.13
RF06	20	1027	45	785	450	100	10.6	5.9	921	0.77	9.28	-3.27	1.13
RF07	24	1138	64	780	510	110	10.5	8.4	921	0.76	9.31	-4.91	1.13
RF08*	25	2240	40	560	325	80	12.5	10.1	944	0.59	10.0	-5.68	1.15
RF08**	25	2643	57	560	325	80	12.5	10.1	944	0.59	10.0	-5.68	1.15
RF09*	27	2132	33	605	270	55	11.8	12.8	944	0.59	9.64	-8.69	1.16
RF09**	27	2422	32	605	270	55	11.8	12.8	944	0.59	9.64	-8.69	1.16
Averages			47	756	360	103	11.6	8.2	935	0.67	9.36	-5.93	1.14

* Afternoon flight segment.

** Evening flight segment.

hole widths by varying 2 degrees of freedom of the distribution, the geometric mean (W_g), and geometric standard deviation (σ_g) of the widths, until a match is found with the frequency distribution of the hole lengths shown in the top panel of Fig. 5. We find $W_g = 7$ m, and $\sigma_g = 3$ m. The frequency distribution of hole lengths generated from the lognormal distribution of hole widths with those parameters is shown as the dashed line (displaced by a factor of 0.2 for clarity) in Fig. 5. The mean value of hole lengths is 20.4 m. This value is significantly smaller than the average hole length of 125 m given by Nicholls (1989) and the 160-m length given by Wang and Albrecht (1994). In both references, the hole lengths are determined by the length of the downdrafts. The main reason for the differences in the mean lengths determined earlier and the present value appears to be the constraint these authors place on their conditional-sampling method where all downdrafts with lengths smaller than $h/20$ were excluded from the length averages. This amounts to ne-

glecting lengths smaller than 19 to 56 m for different Sc flights in Nicholls (1989), and neglecting lengths smaller than 43 m in the one nocturnal flight analyzed by Wang and Albrecht (1994). The obvious effect of such omissions is to produce average lengths significantly greater than the average length for the present data, which uses 4-m horizontal resolution.

The bottom panel of Fig. 5 gives the density of holes as a function of hole length for all the flights. Here

$$N = \sum_{L_1}^{L_2} (\Delta N / \Delta L) \Delta L, \quad (4)$$

where $\Delta L = 4$ m. These distributions show greater variability than the relative distributions in the top of Fig. 5, with the flights with the most vigorous entrainment giving the smallest values of N (see Table 3). The integral of Eq. (4) over all measured lengths for the different flights ranges from about $N = 6$ km⁻¹ to $N = 12$ km⁻¹. These values of N are sensitive to the resolution of the

TABLE 3. Concentration N of holes, percentage p of cloud-free air, and fractional cloud area A_r containing holes for the flight legs at z_a . The entrainment velocity w_e^* at z_a depends on the listed hole fluxes and total water jump at cloud top.

Flight	N (km ⁻¹)	p (%)	A_r	$\Delta q_T \times \rho$ (g m ⁻³)	$\langle w' \rangle$ (m s ⁻¹)	$\langle w' \times LWC' \rangle$ (g m ⁻² s ⁻¹)	$\langle w' \times q_v' \times \rho \rangle$ (g m ⁻² s ⁻¹)	w_e^* (mm s ⁻¹)
RF01	10.0	0.43	0.208	-8.86	-0.102	0.0351	0.0375	-1.93
RF02	11.3	4.78	0.284	-8.94	-0.287	0.0395	0.0327	-2.58
RF03	7.3	0.30	0.167	-8.04	-0.344	0.0662	0.0333	-2.46
RF04	5.7	≈0	0.101	-4.44	-0.544	0.0659	0.0304	-2.41
RF05	12.8	4.15	0.337	-8.09	-0.230	0.0315	0.0373	-3.24
RF06		≈0	0.135	-4.38	-0.345	0.0590	0.0162	-2.62
RF07	6.2	≈0	0.118	-6.31	-0.575	0.0803	0.0482	-2.72
RF08*	11.7	0.55	0.218	-7.06	-0.130	0.0137	0.0107	-0.87
RF08**	7.2	0.87	0.151	-7.06	-0.321	0.0421	0.0271	-1.70
RF09*	9.5	3.16	0.177	-10.6	-0.100	0.0110	0.0006	-0.17
RF09**	11.6	0.29	0.219	-10.6	-0.237	0.0387	0.0040	-1.02

* Afternoon flight segment.

** Evening flight segment.

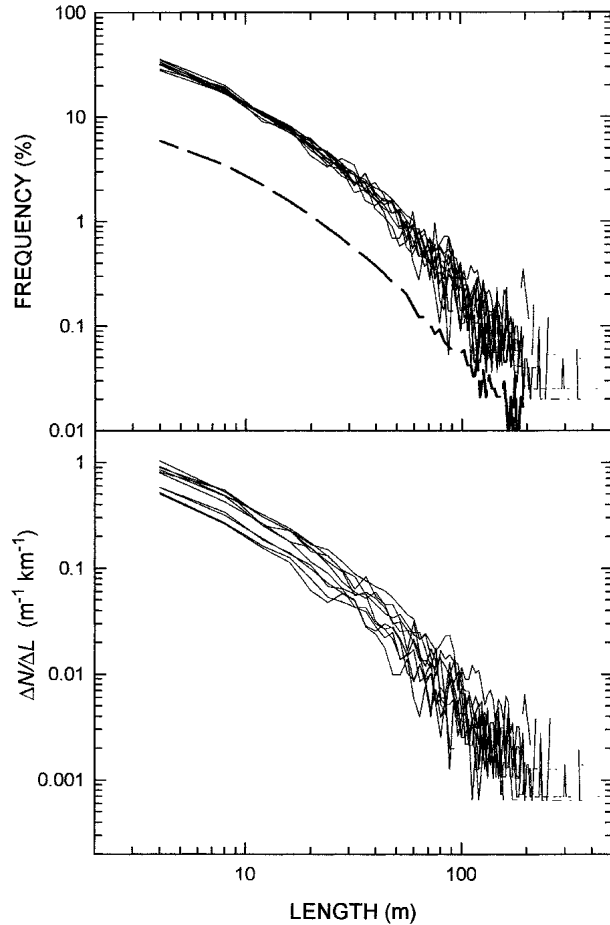


FIG. 5. (top) The frequency distribution of hole lengths for all nine flights measured on average 100 m below cloud top and the best fit dashed curve (shifted for clarity) of lengths derived from a lognormal distribution of widths, and (bottom) the concentration N of holes per kilometer as a function of length for all flights, $\Delta L = 4$ m.

length data. Coarser resolutions than the 4-m resolution used here results in smaller values of N .

Figure 6 gives the frequency distribution of LWC' normalized to the LWC_i at cloud top for two flights. The curves are constructed from LWC' data with an abscissa resolution of 0.01 g m^{-3} . The curve for RF02 is typical of flights with significant cloud-free volumes, and RF07 is typical of flights where only a small number of clear volumes exist.

b. Fluxes and entrainment

Each term of Eq. (3) is evaluated for the flight legs at z_a , and preliminary values of w_e^* are calculated for that flight level. See Table 3 for mean values in the holes of $\langle w' \rangle$, $\langle w' \times LWC' \rangle$, $\langle w' \times (q'_v \times \rho_i) \rangle$, $\Delta q_T \times \rho_i$, and w_e^* . The calculation of q'_v fluxes are limited to the cloud segments defined by the indicator variable LWC' . However, values of $L = 800$ m are used for determining

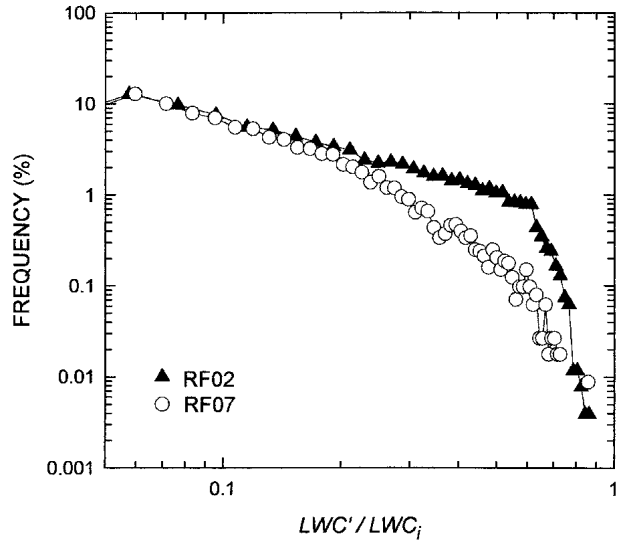


FIG. 6. The frequency distribution of depleted LWC' normalized to LWC_i at cloud top for two flights that differ in the concentration of holes without liquid water.

the horizontal variability of q'_v because the downdrafts are generally cooler than the updrafts and often are larger than the length of the cloud holes, and $K1 = 0.995$ and $K2 = 1.0$ are used because the fluctuations in q'_v are small. The variability of the q'_v flux is small for a range of L , $K1$, and $K2$ values tested about the chosen values. The Lyman-alpha cross-flow hygrometer was used on the aircraft for measuring q'_v .

Table 3 shows that $\langle w' \rangle$ is largest and N is smallest for RF04 and RF07, that LWC' and q'_v fluxes are about the same order of magnitude for the nighttime flights, and that positive values of the q'_v fluxes show that the descending air in the holes has cooled slightly with respect to the upwelling cloudy air. The cooling amount can be calculated using the Clausius–Clapeyron equation, given the assumption that the cloudy air remains at water saturation. The cooling can be a result of two processes: liquid water evaporation due to the entrainment of dryer air, and infrared radiative cooling near cloud top. The relatively constant flux of q'_v versus the variability in the LWC' flux, at least for the first five flights, suggests that IR cooling dominates. This is further supported by the larger flux and w_e^* values in the evening portions of flights RF08 and RF09 in comparison to the daytime portions for which warming by the absorption of shortwave solar radiation has apparently countered much of the IR cooling.

Nicholls (1989) shows from profiling measurements in Sc that the properties of the holes evolve as they are carried along in downdrafts; $|w'|$, T' , $|q'_l|$, $|q'_d|$, A_r , and N get smaller and hole lengths get larger. This behavior is consistent with the mixing of the descending holes with surrounding cloud. Given the trends observed by Nicholls (1989), the w_e^* values in Table 3 obtained from the flight legs at z_a would not be equivalent to the

required cloud-top values of w_e . The average value of w_e^* listed for the nighttime flights in Table 3 is -2.30 mm s^{-1} . This value is smaller than most w_e^* values listed in the literature for measurements done primarily during the daytime (Nicholls and Leighton 1986; Kawa and Pearson 1989; Khalsa 1993; Wang and Albrecht 1994; Wang and Lenschow 1995). The value is also about half the average value of w_e at cloud top given by FAL for the same DYCOMS-II flights, but using different measurement techniques. Thus, the present conditional-sampling method appears to underestimate w_e 100 m below cloud top. The following sections describe the vertical variability of the cloud holes and attempt to extrapolate the w_e^* values to w_e at cloud top.

5. Cloud profiles

The aircraft flew an average of about eight profiles through the Sc on each flight with a profile slant-path slope of about 0.04, which corresponds to about 1.5 min for the typical cloud traverse time. The profiles were dispersed over the entire 6-h flight duration, whereas, the 1-h horizontal legs 100 m below cloud top were flown during the middle of the flight.

Figure 7 shows PVM measurements of 25-Hz LWC for a typical profile. The peak LWC in the profiles averages close to the adiabatic LWC profiles calculated from cloud-base temperatures and pressures. This behavior is also found using LWC measured by the King hot-wire probe on the C-130. Loss of LWC by drizzle precipitation does not appear to play a large role in the DYCOMS-II Sc, some of which contain moderate drizzle. RF02 has the largest drizzle concentration and

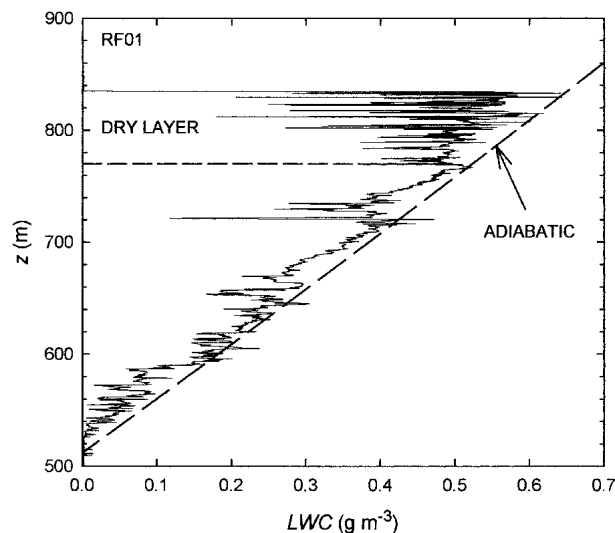


FIG. 7. A typical profile of LWC measured by vertically traversing the Sc layer with the aircraft during RF01. The reduced LWC values in the narrow dry layer near cloud top and the approximate adiabatic behavior of the vertical dependence of LWC is often seen in other profiles.

is closest to the “heavy-drizzle threshold” described by Gerber (1996b). However, LWC in RF02 is also dominated by small droplets, and LWC approaches adiabatic conditions on the average. The largest deviation from adiabatic LWC often occurs in the profiles near cloud top, which has previously been noted for Sc by Nicholls and Leighton (1986). This region is labeled the *dry layer*, and it usually coincides with the greatest concentration of cloud holes, as Fig. 7 shows. The typically small width of the holes suggests that many holes already mix with surrounding cloud near cloud top and cause the reduced LWC. This suggests that the entrainment effects accumulate to some degree in a narrow layer below cloud top, and that with respect to LWC, Sc cannot be assumed to be well mixed.

The conditional sampling of 25-Hz LWC data of all the profiles is used to determine the size of LWC' versus z for which composites are generated for each flight. Figure 8 shows the results for flight RF01, where the largest changes in LWC' are seen near cloud top, and gradual decay of LWC' occurs lower in the cloud. The individual data points in Fig. 8 are averaged for each 10-m height increment, and the averages (circles data) are further given a three-point running mean. An analytical expression can be applied to the mean data by assuming that the size of LWC' decreases with a constant fraction f for each increment of z as z decreases below cloud top. This results in

$$\text{LWC}'(z) = \text{LWC}'(z_i) \times (1 - f)^{(z_i - z)/Z} + \Delta\text{LWC}', \quad (5)$$

where $Z = 1.0 \text{ m}$. The dashed curve in Fig. 8 shows the best fit of Eq. (5) to the mean LWC' data, and the

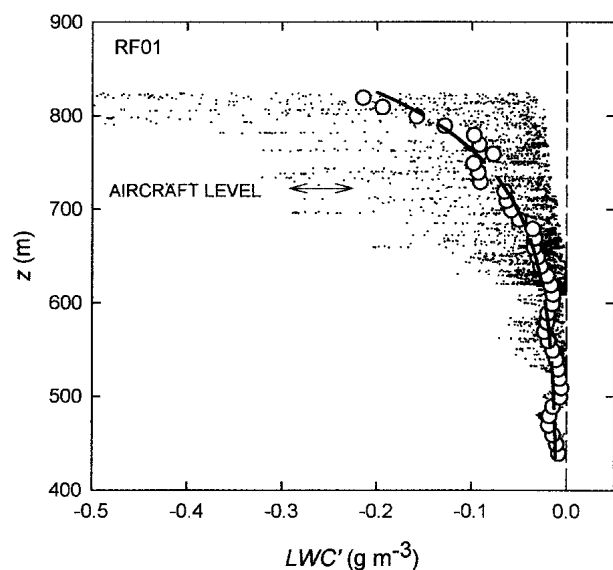


FIG. 8. Composite of eight profiles flown during RF01 showing the amount of depleted LWC' as a function of height in 4-m flight increments (dots), and LWC' averaged over 10-m vertical increments (circles). The dashed curve given by Eq. (5) and numerically described in Table 4 is the best fit to the circles data.

corresponding numerical values for the curve are given in Table 4 for RF01 and the other flights. The values of $LWC'(z_i)$ in Table 4 do not vary greatly which suggests that the geometry of the holes at cloud top is quite similar for all the flights. In addition, the small range of f suggests that the decay of LWC' below cloud top is similar. Another way to treat the LWC' data from the profiles is to calculate the density of LWC' with respect to z , giving $LWC'(z)/\Delta z$. The resulting curves (not shown) are similar in shape but not in amplitude to those described by Eq. (5).

Inspection of $q'_v(z)$ in Sc profiles (not shown) indicates that the absolute value of $|q'_v(z)|$ decreases more gradually with decreasing z than the absolute value of $|LWC'(z)|$. The largest differences are found near cloud top where $|q'_v(z)|$ appears to decrease with height over a thin layer rather than showing the sharp increase of $|LWC'(z)|$ in the same location. Given the large fluctuations of $q'_v(z)$ near cloud top, the decrease in $|q'_v(z)|$ is difficult to illustrate for most flights. The decrease is best seen in the composite shown in Fig. 9 of the last six profiles flown during the evening of flight RF09 (from 2324 to 2620 UTC) which had the greatest buoyancy jump at the inversion of all the flights, probably causing a flatter cloud top. Figure 9 shows that $|q'_v(z)|$ decreases over about a 30-m-thick layer adjacent to cloud top. This result indicates that the temperature in the holes at cloud top differs little from the adjacent unaffected cloud, and that cooling due to IR flux divergence develops over a finite layer.

The profiles also lend themselves to finding the dependence of the hole area ratio A_r on z . Figure 10 gives the composite of A_r for all the profiles of each flight translated vertically to a common cloud-top height of $z = 700$ m, with the curves resulting again from averaging the 25-Hz LWC data over 10-m increments and then using a 3-point running mean. Not all flights are represented in Fig. 10 for the sake of clarity. The typical shape of the curves in Fig. 10 is hypothesized to be a

TABLE 4. Parameters of Eq. (5) that describe the change of depleted LWC' in the holes as a function of height in the Sc. Here, R1 and R2 are constants used to scale w_e^* measured at z_a to w_e at cloud top.

Flight	f	$\langle LWC'(z_i) \rangle$ ($g\ m^{-3}$)	$\Delta LWC'$ ($g\ m^{-3}$)	R1	R2
RF01	0.0120	-0.190	-0.010	1.34	1.40
RF02	0.0135	-0.170	-0.028	1.36	1.21
RF03	0.0150	-0.220	-0.028	1.84	1.80
RF04	0.0140	-0.260	-0.035	3.71	1.38
RF05	0.0140	-0.210	-0.016	1.11	2.12
RF06	0.0100	-0.240	-0.025	3.19	1.27
RF07	0.0170	-0.230	-0.050	2.59	1.34
RF08*	0.0200	-0.195	-0.020	2.02	1.18
RF08**	0.0200	-0.195	-0.020	2.91	1.18
RF09*	0.0210	-0.205	-0.025	1.60	1.23
RF09**	0.0210	-0.205	-0.025	1.29	1.23

* Afternoon flight segment.
 ** Evening flight segment.

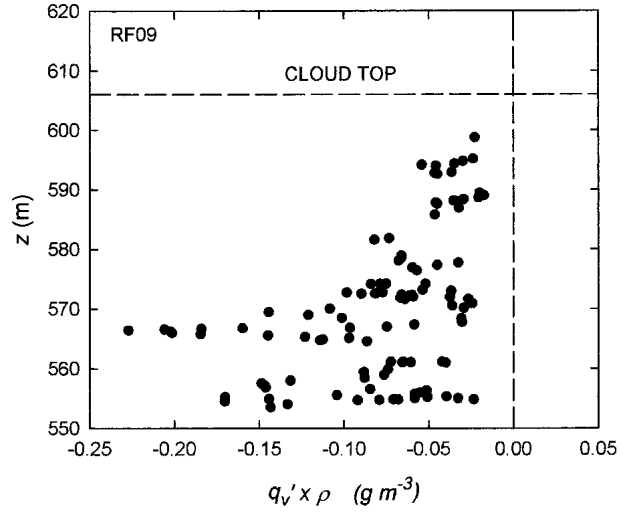


FIG. 9. Composite of the depleted water vapor content in holes as a function of height near cloud top determined from Sc profiles made during the evening portion of flight RF09.

result of the following: Near cloud top, the area covered by the holes dominates A_r , the area rapidly decreases as the holes mix with the surrounding cloud in the descending air, and the increase in A_r at lower levels in the Sc is due to the greater effect descending air from the dry layer has as it approaches its *sinking evaporation level* (SEL). The heights of SEL will be greater than LCL and are the likely reason for the large variability of cloud base often observed in Sc. The ratio $R1 = A_r(z_i)/A_r(z_a)$ uses A_r determined from cloud-top and aircraft-level data in Fig. 10 and is listed in Table 4.

A similar procedure is followed for each flight to obtain the ratio R2 between the fluxes of LWC' and q'_v (Figs. 11a,b) at cloud top and at aircraft level. Figure 11c gives the sum of the LWC' and q'_v fluxes to which a least squares straight line is fitted. Then R2 is found using the solid circles in Fig. 11c, and R2 values are listed in Table 4. Given the short traverse time of the aircraft for each profile, it is not possible to use a lengthy averaging distance for L_w . Here, $L_w = 0.8$ km is used, which will tend to underestimate the fluxes as shown in Table 1.

A final compilation of the profiles data is shown in Fig. 12 where the relative LWC' flux is given versus the length of the holes with a resolution of 4 m. Holes found in the top 50 m of all profiles are used to compile the Fig. 12 circles data, which are given a three-point running mean to generate the given curve. The curve suggests that the mean hole length transporting the mean LWC' flux is no larger than about 20–40 m, or that the mean hole width, given the previous discussion, is only about $1/3$ as large. Those hole sizes may still be an overestimate and the measured LWC' fluxes an underestimate because the relatively large separation between the PVM located outboard on one wing of the C-130 and the gust probe on the aircraft's nose will

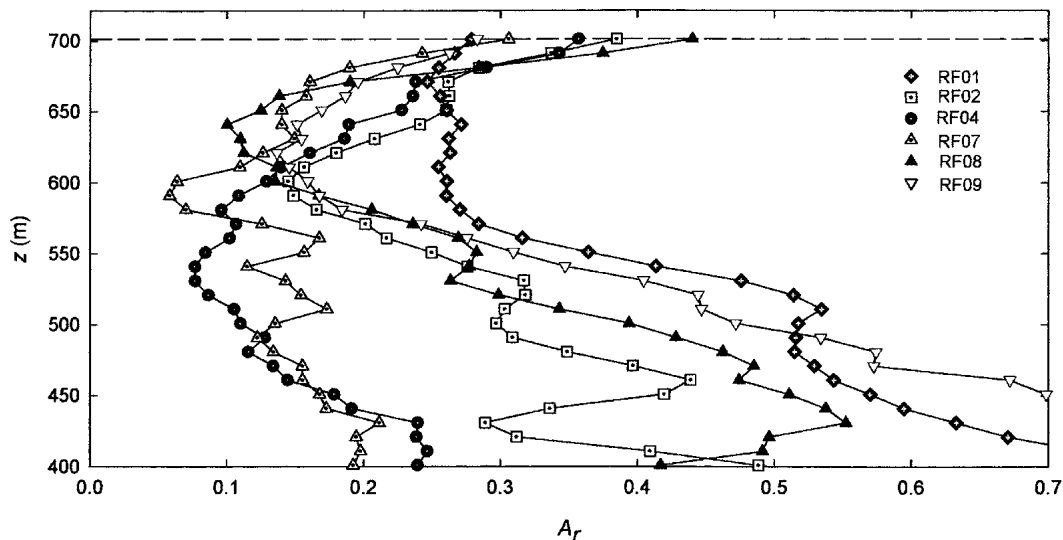


FIG. 10. Composite curves derived from all profiles from each flight of the vertical dependence of the hole area ratio A_r .

cause the contribution of smaller holes to be underestimated in an unknown fashion.

6. Entrainment velocity

The average entrainment velocity w_e at cloud top during the nominal 1-h flight at z_a is calculated for each

flight by using $w_e = R1 \times R2 \times w_e^*$. The values of each w_e and its sample standard deviation s are listed in Table 5, and shown in Fig. 13, with error bars given by $\pm s$. The usual method of random error propagation is used to calculate s given measures of the variability of A_r , w_e^* , Δq_T , R1, and R2 during the 1-h flight period for the first three parameters, and for all the profiles for the

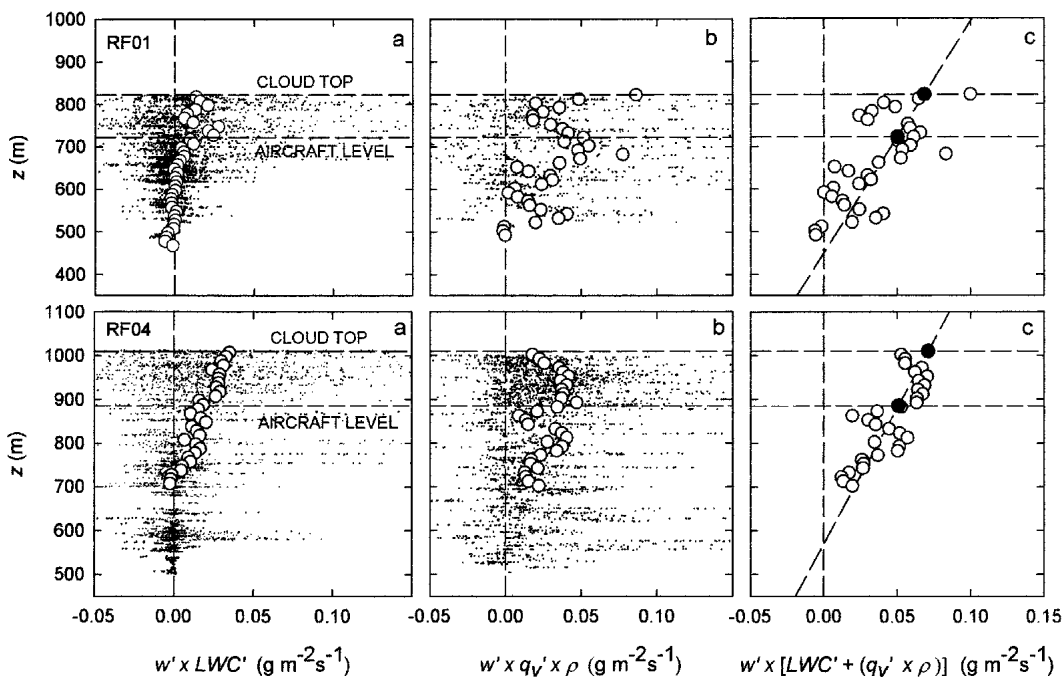


FIG. 11. Composite data of the vertical dependence of (a) LWC' and (b) q_v' fluxes determined from all profiles for flights RF01 and RF04. (c) Sum of the fluxes and a least squares straight line from which the ratio of the fluxes at cloud top and aircraft level (solid circles) are determined to give the value of R2 listed in Table 4. The dots are 4-m resolution data, and the circles are averages over 10-m vertical increments.

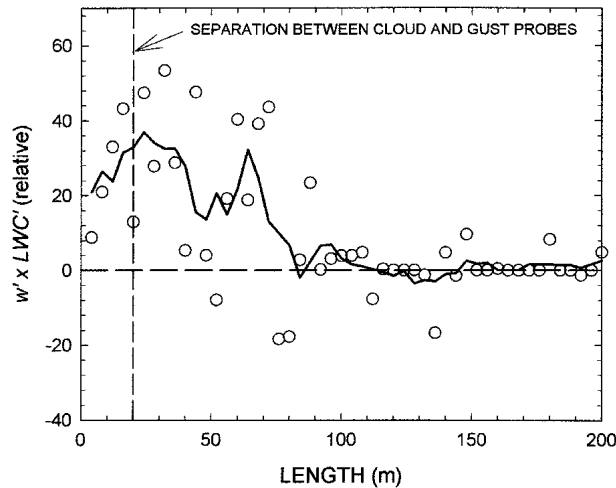


FIG. 12. Composite of the relative flux of LWC' as a function of hole length (horizontal resolution of 4 m) for the top 50 m of all cloud profiles. The solid line is a running average of the individual data points.

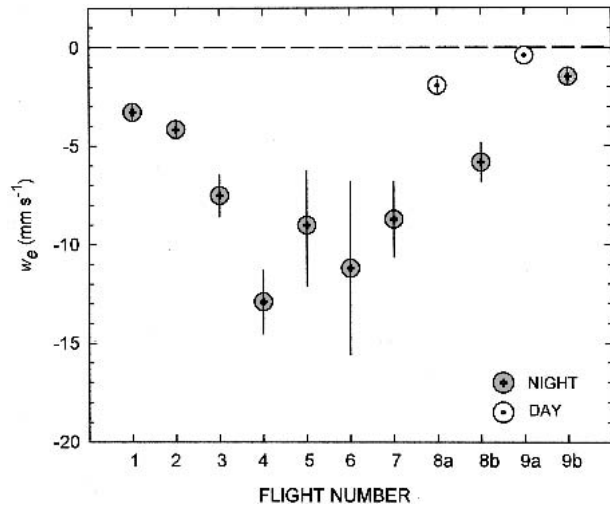


FIG. 13. Average entrainment velocity w_e at cloud top for the nominal 1 h that the aircraft flew about 100 m below cloud top (see Table 2).

last two parameters. As shown, the values of R1 and R2 listed in Table 5 have a substantial effect on increasing w_e^* , with w_e values on the order of 10 mm s^{-1} resulting for some of the flights. The difference in Fig. 13 between w_e in the evening and afternoon portions of flights RF08 and RF09 is large; the ratios of w_e for the portions are 3.02 and 3.66, respectively. Figure 14 further illustrates this difference by showing 20-km segments of LWC measured at z_a and in the same general geographical location during the afternoon and evening portions of RF09. While the average LWC is about the same for both portions, the difference in the density and amplitude of the holes is apparent. Nicholls and Turton (1986) give w_e values for night and daytime flights in Sc, but do not show such large differences, which may be a result of their flights being held on different days.

The cloud-top values of w_e in Table 5 should com-

pare best with the earlier values of w_e in Sc determined by Nicholls (1989), Khalsa (1993), and Wang and Albrecht (1994), because those values of w_e were also obtained using the conditional sampling method. Of this earlier work, the results from Wang and Albrecht (1994), who found $w_e = -4.9 \text{ mm s}^{-1}$, may be the most

TABLE 5. Values of the entrainment velocity w_e and their std dev s at cloud top, potential temperature jumps at cloud top, and the entrainment stability factor κ .

Flight	w_e (mm s^{-1})	s	$\Delta\theta_v$ ($^{\circ}\text{K}$)	κ	$\Delta\theta_e$ ($^{\circ}\text{K}$)
RF01	-3.28	-0.459	8.74	0.55	-9.6
RF02	-4.16	-0.447	6.08	0.74	-12.5
RF03	-7.51	-1.08	6.50	0.63	-9.0
RF04	-12.9	-1.62	5.61	0.32	-2.9
RF05	-9.02	-2.93	5.15	0.89	-15.2
RF06	-11.2	-4.39	5.49	0.34	-2.9
RF07	-8.71	-1.92	7.77	0.38	-4.7
RF08*	-1.93	-0.315	9.30	0.38	-5.1
RF08**	-5.82	-1.01	9.30	0.38	-5.1
RF09*	-0.404	-0.102	11.5	0.51	-10.0
RF09**	-1.48	-0.358	11.5	0.51	-10.0

* Afternoon flight segment.

** Evening flight segment.

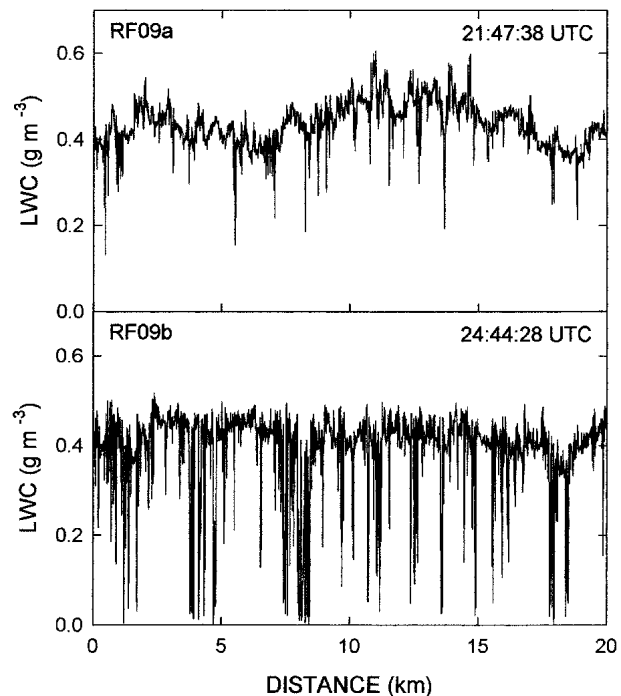


FIG. 14. LWC for a 20-km stretch of horizontal flight through Sc during the (top) afternoon and (bottom) evening of flight RF09. Both parts were flown in the same general area off the California coast.

comparable because they also analyze a nocturnal Sc off the California coast. Khalsa (1993) finds $w_e = -0.64$ and -1.99 mm s^{-1} for daytime Sc, and Nicholls (1989) states that his conditional-sampled w_e values are “consistent” with values (ranging from -2.4 to -7.1 mm s^{-1}) established by other means and referenced in Nicholls and Leighton (1986). While all these preceding values of w_e fall within the range of w_e values given in Table 5, it is obviously difficult to justify such a comparison simply because the measurements were made at different times and for different clouds. However, using other results already presented here, we can speculate that these earlier w_e measurements in Sc likely underestimated actual w_e values for the following reasons: First, in all the earlier work the flight level for which w_e was determined was below cloud top [50 m for Nicholls (1989), 90 m for Wang and Albrecht (1994), 100 m for Khalsa (1993)], and no scaling was done to estimate cloud-top w_e values. Given the sharp gradients in entrainment fluxes illustrated in Fig. 11, the lack of such scaling would cause w_e underestimation at cloud top. Second, neglecting scales of the entrainment holes up to about 50 m in length, as done in the conditional sampling method used by Nicholls (1989) and Wang and Albrecht (1994), would cause substantial loss of entrainment flux, which affects the magnitude of w_e , as illustrated in Fig. 12. And third, the preceding authors also set a rule wherein downdrafts smaller than about 0.4 m s^{-1} were not included in the conditional sampling, causing potentially further reduction of w_e values. It is not possible to establish accurately how much underestimation of w_e is caused by those three sources—perhaps as much as a factor of 2 is needed to correct those underestimates.

Inspection of the parameters listed in Tables 3 and 5 shows that w_e for the night flights is most strongly correlated to the temperature jump ΔT across the inversion, and to the closely related virtual potential temperature jump $\Delta\theta_v$ listed in Table 5. Figure 15 relates $\Delta\theta_v$ and w_e showing that a monotonic relationship exists approximately between the two variables, with the absolute value of w_e decreasing more rapidly than an inverse proportionality with $\Delta\theta_v$ would indicate. The equation for the least squares line applied to the conditional-sampling data in Fig. 15 is $w_e \text{ (mm s}^{-1}\text{)} = 1.15 \text{ (mm s}^{-1} \text{ K}^{-1}\text{)} \Delta\theta_v \text{ (K)} - 18.8 \text{ (mm s}^{-1}\text{)}$. The data also suggest that at about a value of $\Delta\theta_v = 13 \text{ K}$ entrainment should cease. A monotonic relationship should be expected under the conditions that convection in the nighttime, mostly unbroken Sc is forced by relatively constant radiative cooling and that the magnitude and variability of other processes that contribute to the convection in such Sc are small. Large error bars in the measured w_e values require that the monotonic relationship is considered tentative.

Figure 15 also shows w_e values derived by applying the flux-jump method to data from the same DYCOMS-II flights (FAL). The FAL values in Fig. 15

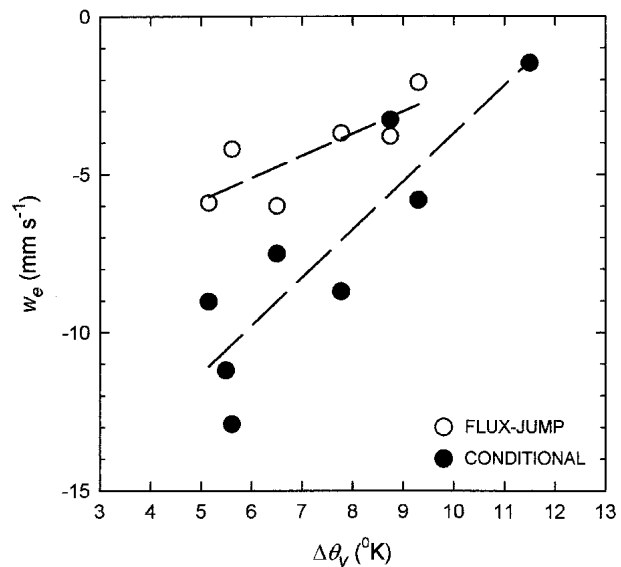


FIG. 15. Comparison of entrainment velocity and buoyancy jump across cloud top for DYCOMS-II flights measured with the flux-jump approach (data from FAL) and with the present approach using conditional sampling of cloud holes. Lines are least squares fits.

are averages of w_e values calculated using the three scalars: DMS, ozone, and q_T . Comparing the two w_e datasets is inherently difficult because the flux-jump measurements were made over most of the 6-h duration of the flights at the Sc sites, whereas the conditional method only uses the nominal 1-h interval near the middle of the flights. The two w_e datasets differ by a factor of about 1.9. The w_e measurements based on DMS agree better with the present measurements of w_e than those based on ozone and q_T . The best agreement of the average w_e is found between the present w_e values and w_e values constructed by adding the subsidence rates calculated in FAL with the rise of cloud top determined here for the first seven nocturnal flights. The average rise for those flights, 3.6 mm s^{-1} with a standard deviation of 2.7 mm s^{-1} , is established by fitting a least squares straight line to cloud-top height values observed during the flights using the aircraft profiles and 1-Hz-averaged LWC data. It is of interest to note that the two measurement techniques differ significantly in the cloud scales most important to the respective w_e measurements. For the flux-jump approach about 1 km is shown to be the dominant scale (FAL), while about 10 m is the dominant scale for the conditional approach. The latter has the disadvantage of dealing with sharp gradients of the entrainment-depleted quantities near cloud top, but does not share with the former the requirement of measuring w deviations from the adjusted mean w value with accuracy requirements that are several orders of magnitude more stringent.

7. Entrainment stability

The omnipresence of cloud holes with depleted LWC' observed in all of the DYCOMS-II flights is related to the oft-deliberated question: What is the role in the entrainment process of air cooled by cloud water evaporation? Lilly (1968), Randall (1980), and Dearnorff (1980) hypothesized that this cooling could cause buoyancy instability at cloud top under certain conditions affecting the entrainment rate and potentially speeding the breakup of Sc. The criterion for this cloud-top entrainment instability (CTEI) is given by

$$\Delta\theta_e < \kappa \frac{L}{c_p} \Delta q_T, \quad (6)$$

where $\Delta\theta_e$ is the equivalent potential temperature between cloud top and the free atmosphere, L is the latent heat of evaporation, c_p is the specific of air at constant pressure, and the stability parameter κ is given a value 0.23 that corresponds to the dividing line between stable ($\kappa < 0.23$) and unstable cloud top ($\kappa > 0.23$). Other related criteria are described by Shy and Bretherton (1990) and Duynkerke (1993).

Observations that tested the CTEI criterion (e.g., Kuo and Schubert 1988; Siems et al. 1990) have not supported this concept. Albrecht et al. (1985) suggested that CTEI would not hold if entrainment caused the entire liquid water in a mixing parcel to evaporate, and Siems et al. (1990) and Wang and Albrecht (1994) indicated that only specific and possibly rare mixing mass fractions [$\varepsilon = m_a/(m_a + m_c)$] of free atmosphere (m_a) and cloudy air (m_c) would lead to potential destabilization. However, some recent Sc modeling (Lewellen and Lewellen 1998; Moeng 2000; also see comments in Stevens et al. 2003b) has supported the CTEI concept.

The values of $\Delta\theta_e$ and κ are calculated from profiles of each DYCOMS-II flight and are listed in Table 5. All κ values indicate that these Sc should tend toward breakup. Instead, the Sc remained unbroken and with cloud thickness generally increasing. Further, no correlation is seen in Table 5 between κ and w_e .

In searching for reasons for the consistent disagreement between CTEI and the earlier and present observations we look at the 1000-Hz UFT and PVM data and the 50-Hz FFSSP data collected during shallow porpoising of the aircraft between about 50 m above and below cloud top during RF03. (While such porpoising was done on most flights, RF03 was judged to give the most reliable UFT temperature data, which compared well in and out of cloud with the Rosemont reverse-flow probe temperature data collected at a slower rate). Figure 16 shows the gradual descent of the aircraft into the top of the Sc during a short interval of the porpoising. The major features of Fig. 16 are 1) the cloud holes, 2) the EIL, where the temperature of cloud-free air is between the steady in-cloud temperature and the 7.5°C warmer temperature of the free atmosphere above the

EIL, and 3) the location where submeter-scale mixing is apparently taking place. The FFSSP shows that the droplet spectra changes a minimal amount in the holes except for feature 3, where all the droplets should evaporate because the final temperature after mixing is complete will be about 0.7°C warmer than the cloud. The EIL has an average thickness of 22 m during the porpoising part of RF03. The moistening and cooling of the EIL with cloudy air has been noted previously (Caughey et al. 1982; Nicholls and Turton 1986; Gerber 1996a; Brenguier et al. 2000; Lenschow et al. 2000; VanZanten and Duynkerke 2002); however, the relationship of this process to entrainment into the cloud has remained unclear. While some vigorous convective updrafts must penetrate the EIL to engulf some air from the free atmosphere, the sequence of mixing events following the initial penetration and leading to entrainment into cloud top is poorly understood. Wang and Albrecht (1994) calculated that mixing cloud-top air with air from decreasing levels in the EIL resulted on average in larger ε values that tended to totally evaporate liquid water in the mixtures. Thus, if air at EIL levels close to cloud top mixes predominantly with the cloud [akin to the mechanism proposed by MacVean and Mason (1990)] evaporative cooling and the entrainment instability will tend to be minimal, while on the other hand, mixtures from highest EIL levels and largest temperature differences would maximize the evaporative cooling effect. The temperatures in the EIL shown in Fig. 16 suggest that the actuality may lie somewhere in between those extremes. To estimate where this may be, conditional sampling of LWC' and T' in holes is done for the porpoising section of RF03 using the 10-cm resolution data. Figure 17 shows the composite of LWC' and T' for 39 holes for which lengths (mean length of 12.1 m) are normalized to a constant relative distance, and the LWC values are normalized to the overall LWC average outside of the composite hole. The average temperature difference between the composite hole and the adjacent portions is -0.019°C . Interpretation of the measured temperature difference between holes and adjacent clouds is made more difficult by the probes being separated laterally on the aircraft wing by 6.2 m. In contrast, mixing line analysis predicts a maximum cooling of -0.15°C if all the liquid water is evaporated in a mixed parcel consisting of cloud-top and free atmosphere air. Given that the LWC' depletion in Fig. 17 averages about half the average LWC value outside of the composite hole, the measured cooling is about 25% of the average maximum cooling of -0.075°C . Unfortunately, it is not possible to claim that this cooling is a result only of evaporative cooling because the aircraft flew at an average level of 18.3 m below cloud top as estimated from the 10 cloud penetrations made during the porpoising. Thus, radiative cooling could also be the cause of the measured cooling as suggested by Fig. 9. Still, these results

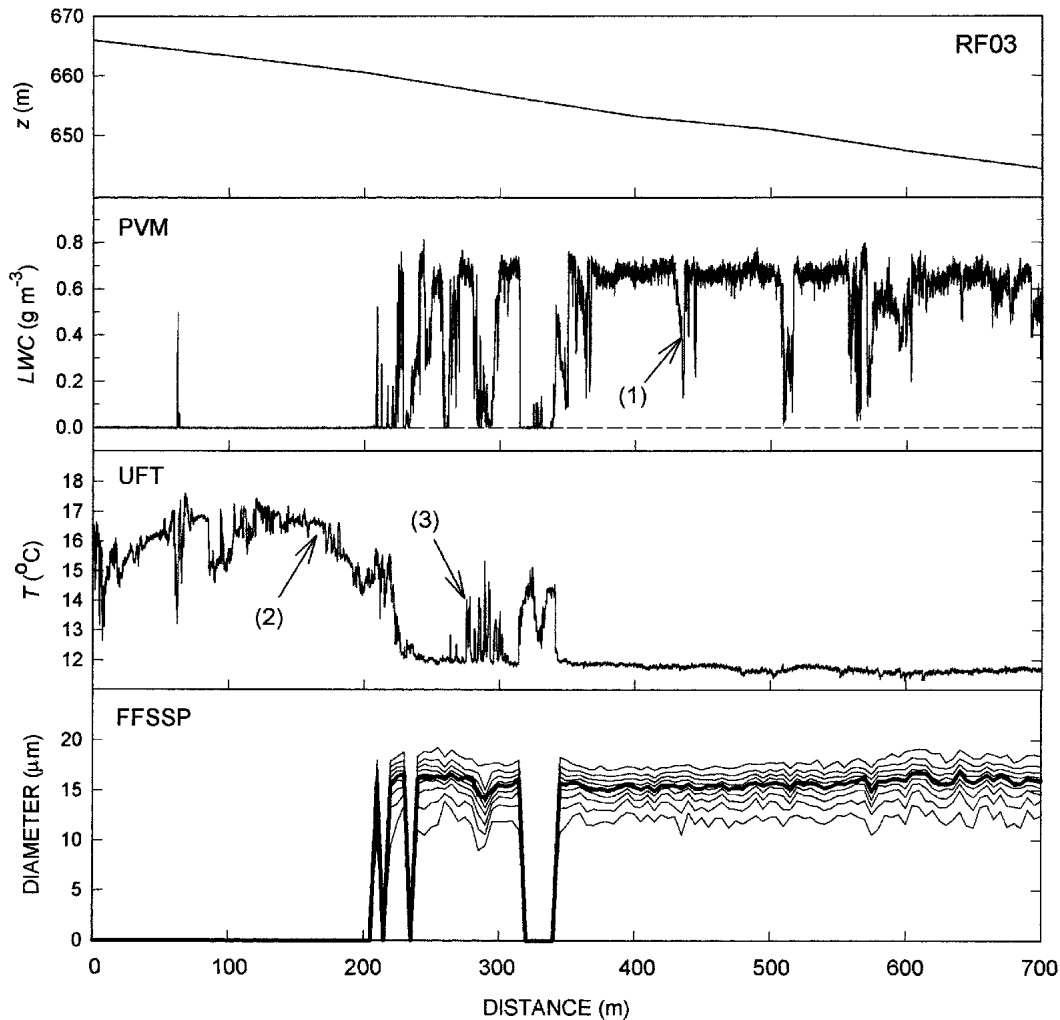


FIG. 16. (top) Gradual descent of the aircraft into cloud top during RF03 showing 1000 Hz (~ 10 cm spatial resolution) PVM and UFT and 50-Hz FFSSP (~ 2 m resolution) measurements. The thin lines in the FFSSP data are 10% percentiles of the droplet concentration, and the thick line gives the mass median diameter. One of the holes with depleted LWC is indicated by “(1)”; temperatures in the entrainment interface layer by “(2)”; and a region with finescale mixing by “(3)” [from Gerber et al. (2002) with changes].

suggest that evaporative cooling plays a minimal role in RF03 even though buoyancy reversal is predicted given the large value of κ . We hypothesize that detrainment of cloud causes conditioning of the EIL with multiple mixing events until a buoyancy match is approached with cloud top. At that point, air is entrained into cloud top in a nearly isothermal fashion from primarily low levels of the EIL, causing inhomogeneous mixing that dilutes the droplet concentration but leaves the spectra mostly unaffected, as shown in the bottom panel of Fig. 16. The CTEI criterion appears to fail because it deals with the entire cloud-top jumps and not with the details of mixing between the EIL and the adjacent air.

Thus the possibility exists that evaporation of LWC at the top of this Sc contributes primarily to cooling the EIL by a small amount, whereas the holes enter cloud

top in a thermodynamically passive way and are carried away and downward in the larger eddy circulation caused by radiative cooling. Krueger (1993) pointed out that mixing of the holes with the adjacent cloud and the associated buoyancy instability was not limited only to cloud top, but continued as the holes were drawn downward into the cloud. Wang and Albrecht (1994) further discuss this scenario. The present work supports these possibilities, showing that holes can penetrate hundreds of meters downward into the Sc before most are lost by mixing with adjacent clouds. The key question to ask is whether the rate of mixing of the holes with adjacent clouds is fast enough that the holes do not reach their SEL. If they do, which appears possible given the small LWC in some holes at cloud top, the continuing descent of the holes will be dry adiabatic generating more tur-

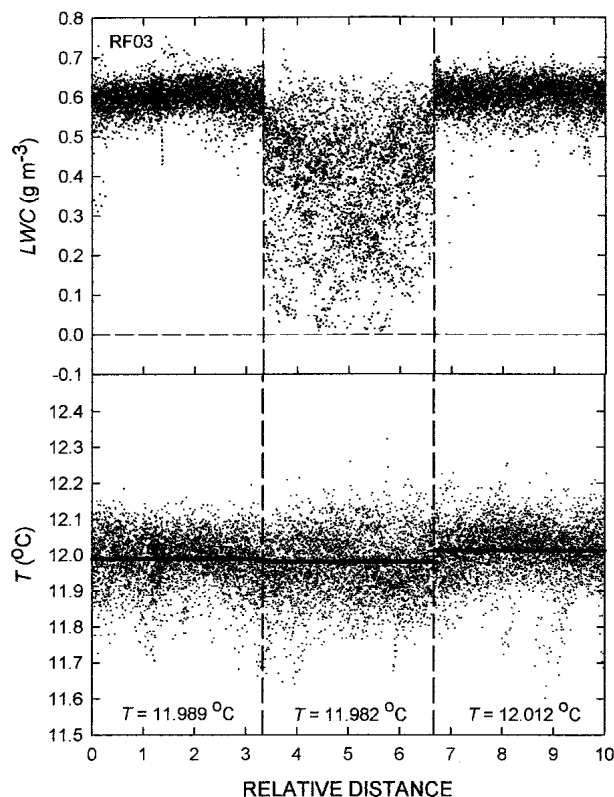


FIG. 17. Composite of 1000-Hz conditionally sampled LWC and average temperature (T ; °C) data in cloud holes and adjacent areas from the aircraft porpoising section at cloud top for RF03. The hole lengths are normalized to the same relative distance bordered by the vertical dashed lines.

bulence and mixing, and enhancing convection by additional evaporative cooling. A search of the UFT data for RF03 was made for parcels with such a cloud interior mixing instability (CIMI) with minimal results. The UFT data are too sparse to draw conclusions, even though a few holes in the cloud interior with both cooling and warming were found. The application of the linear eddy mixing model (Krueger 1993) including implicit microphysics and dynamic feedback appears well suited for exploring CIMI. In the process of looking at UFT data in the Sc interior, some holes were found with temperature differences with the adjacent cloud of as much as -0.4°C , again showing that cloud-top evaporative cooling was negligible in comparison to cooling that was most likely dominated by IR flux divergence near cloud top.

8. Summary and conclusions

The description of cloud holes, including the areal coverage of holes at cloud top, the change of hole size with height in the cloud, and the decrease of the magnitude of the depleted LWC' and of the flux $w' \times \text{LWC}'$ in the holes with increasing distance below

cloud, are in general agreement with the conditional sampling results of Nicholls (1989). We used newer instrumentation that permitted characterization of the holes with greater resolution than previously possible. Both the present analysis of flight RF03 and that by Nicholls (1989) of a mixture of daytime and nighttime Sc conclude that cooling in the Sc due to liquid water evaporation at cloud top caused by entrainment is significantly smaller than the cooling generated by IR flux divergence near cloud top. In contrast, Wang and Albrecht (1994) find both cooling amounts to be of similar magnitude in a nocturnal Sc also off the West Coast.

The cloud holes containing water depleted by entrainment are readily identifiable in all of the nine DYCOMS-II flights in Sc. The average characteristics of the holes are as follows: the aircraft penetration length of holes is about 20 m at 100 m below cloud top and is about 12 m at cloud top; the width of holes is 7 m at 100 m below cloud top and about 5 m at cloud top; the relative frequency distribution of hole lengths is nearly constant for all flights; the average concentration N along the horizontal flight path of holes greater than 4 m in length ranges from about 6 to 12 holes km^{-1} , with Sc with the highest entrainment rate showing reduced values of N and at the same time showing the largest values of downdraft velocity in the holes; the decrease in size of LWC' values with distance below cloud base can be well represented by an expression that assumes that a constant fraction of the values is lost for every height increment, and the holes penetrate as much as hundreds of meters deep in Sc with the most vigorous entrainment before the holes are lost by mixing.

The values of the entrainment velocity w_e estimated from measurements made during nominal 1-h horizontal flights about 100 m below Sc top are judged to underestimate w_e values at cloud top, because w_e depends on the areal coverage of the holes and the fluxes of depleted LWC' and $q'_{v'}$, which change rapidly with height near cloud top. Data from aircraft profiling are used to scale w_e to cloud top using measurements of the vertical dependence of coverage and fluxes.

Earlier measurements (Nicholls 1989; Khalsa 1993; Wang and Albrecht 1994) of w_e for Sc using conditional sampling of cloud holes likely underestimate w_e values by significant amounts because the rapid changes of entrainment fluxes found near cloud top are not taken into account, and because the minimum entrainment scales applied in those studies are not small enough to capture a large portion of the entrainment fluxes as shown by the higher-resolution data used here. The present measurements of w_e are a factor of 1.9 larger on average than the measurements of w_e made on the same DYCOMS-II flights and reported by FAL.

The dominant hole length for transporting entrainment flux at cloud top is estimated to be about 30 m, and the dominant width is estimated as about 10 m. The separation between the cloud probes outboard on a

wing and the gust probe on the C-130 nose is about 20 m, preventing better estimates of the dominant length and width. This separation and the quality of the gust probe data, which falls off above 10 Hz suggest that the w_e values determined with the present conditional-sampling method may still underestimate the true w_e values.

The average w_e values for the night flights correlate best with the buoyancy jumps above cloud top. A monotonic relationship exists between w_e and the buoyancy jump; however, the error bars for the w_e values are large, suggesting a tentative relationship.

The entrainment stability parameter κ is in the unstable range for the Sc from all flights predicting that thinning and breakup of the Sc should occur, but which does not occur. This result is consistent with previous similar studies. The nocturnal Sc in DYCOMS-II mostly thicken, and no correlation is found between κ and the entrainment rate. The existence of robust nocturnal Sc during DYCOMS-II with relatively large values of the entrainment rate suggests that the value of the entrainment rate is a necessary but not a sufficient condition for the thinning and breakup of these nocturnal Sc. Well-developed convection caused by radiation cooling apparently provides the mechanism for efficiently transporting water vapor into the cloud from the ocean surface to more than replenish liquid water lost by entrainment drying. Solar heating of the Sc is the likely cause for decreasing the entrainment rate by a factor of about 3 during the afternoon portions, in comparison to the evening portions of flights RF08 and RF09. The large amount of drizzle found in RF02 may also reduce convection as a result of stability caused by the cooling of evaporating drizzle below cloud base, or by directly affecting updraft velocity given that drizzle is found predominantly in the updraft of the Sc, as found previously for other drizzling Sc (Vali et al. 1998).

The small temperature difference between the holes and the adjacent unaffected cloud at cloud top, the inhomogeneous nature of mixing that produces the holes in the cloud at cloud top, and the existence of the entrainment interface layer (EIL) above cloud suggest that clouds are detraining to condition by cooling the cloud-free EIL until a near-buoyancy match is achieved between the EIL and the cloud, at which point air is entrained into the cloud. It is not possible to identify the mechanism by which air is ultimately entrained, or the scales that come into play in the mixing between the free atmosphere, the EIL, and the cloud, given the inadequate data resulting primarily from insufficient collocation on the aircraft of the gust, microphysical, and temperature probes, and from the lack of time the aircraft spend near the thin EIL.

The deployment and data generated during DYCOMS-II by the fast probes, UFT, PVM, and FFSSP, on the C-130 was a learning experience that can benefit future use of these probes. Better collocation of

the probes with a gust probe is essential if features as small as cloud holes and their cloud interactions are to be reliably studied. The gust probe should have a response of at least 50 Hz. Much more aircraft time should be spent within 50 m of cloud top, especially if conditional sampling of holes in Sc is repeated to improve measurement accuracy and understanding. A slow aircraft should be used, or better yet, a motorized airship with probes suspended underneath should be used as proposed earlier (Gerber 1996a).

Acknowledgments. Appreciation is expressed to the Research Aviation Flight facility of NCAR for their dedicated and excellent effort during the DYCOMS-II experiment. Thanks are due Bjorn Stevens and Donald Lenschow for organizing DYCOMS-II. One of us (H.G.) was supported by the National Science Foundation (Grant ATM-0107738).

REFERENCES

- Albrecht, B. A., R. S. Penc, and W. H. Schubert, 1985: An observational study of cloud-topped mixed layers. *J. Atmos. Sci.*, **42**, 800–822.
- Brenguier, J.-L., T. Bourrienne, A. A. Coelho, J. Isbert, R. Peytavi, D. Trevarin, and P. Weschler, 1998: Improvements of droplet size distribution measurements with the Fast-FSSP. *J. Atmos. Oceanic Technol.*, **15**, 1077–1090.
- , H. Pawlowska, L. Schueller, R. Preusker, J. Fisher, and Y. Fouquart, 2000: Radiative properties of boundary layer clouds: Droplet effective radius versus number concentration. *J. Atmos. Sci.*, **57**, 803–821.
- Caughey, S. J., B. A. Crease, and W. T. Roach, 1982: A field study of nocturnal stratocumulus: II. Turbulence structure and entrainment. *Quart. J. Roy. Meteor. Soc.*, **108**, 125–144.
- Deardorff, P. G., 1980: Cloud-top entrainment instability. *J. Atmos. Sci.*, **37**, 131–147.
- Duroire, C., and B. Guillemet, 1990: Analyse des heterogeneites spatiales des stratocumulus et cumulus. *Atmos. Res.*, **25**, 331–350.
- Duynkerke, P. G., 1993: The stability of cloud top with respect to entrainment: Amendment of the theory of cloud top entrainment instability. *J. Atmos. Sci.*, **50**, 495–502.
- Gerber, H., 1996a: Microphysics and modeling of layer clouds. *Proc. ETL/CSU Cloud Modeling and Measurement Workshop*, Boulder, CO, National Oceanic and Atmospheric Administration, 175–187.
- , 1996b: Microphysics of marine stratocumulus clouds with two drizzle modes. *J. Atmos. Sci.*, **53**, 1649–1662.
- , B. G. Arends, and A. S. Ackerman, 1994: A new microphysics sensor for aircraft use. *Atmos. Res.*, **31**, 235–252.
- , S. P. Malinowski, J.-L. Brenguier, and F. Burnet, 2002: On the entrainment process in stratocumulus clouds. Preprints, *11th Conf. on Cloud Physics*, Ogden, UT, Amer. Meteor. Soc., CD-ROM, JP7.6.
- Haman, K. E., S. P. Malinowski, B. Strus, R. Busen, and A. Steffen, 2001: Two new types of ultra-fast aircraft thermometer. *J. Atmos. Oceanic Technol.*, **18**, 117–134.
- Kawa, S. R., and R. Pearson Jr., 1989: An observational study of stratocumulus entrainment and thermodynamics. *J. Atmos. Sci.*, **46**, 2649–2661.
- Khalsa, S. J. S., 1993: Direct sampling of entrainment events in a marine stratocumulus layer. *J. Atmos. Sci.*, **50**, 1734–1750.
- Korolev, A. V., and I. P. Mazin, 1993: Zones of increased and decreased droplet concentration in stratiform clouds. *J. Appl. Meteor.*, **32**, 760–773.

- Krueger, S., 1993: Linear eddy modeling of entrainment and mixing in stratus clouds. *J. Atmos. Sci.*, **50**, 3078–3090.
- Kuo, H. C., and W. H. Schubert, 1988: Stability of cloud-topped layers. *Quart. J. Roy. Meteor. Soc.*, **114**, 887–916.
- Lenschow, D. H., M. Zhou, X. Zeng, L. Chen, and X. Xu, 2000: Measurements of fine-scale structure at the top of marine stratocumulus. *Bound.-Layer Meteor.*, **97**, 331–357.
- Lewellen, D., and W. Lewellen, 1998: Large-eddy boundary layer entrainment. *J. Atmos. Sci.*, **55**, 2645–2665.
- Lilly, D. K., 1968: Models of cloud-topped mixed layers under a strong inversion. *Quart. J. Roy. Meteor. Soc.*, **94**, 292–309.
- MacVean, M. K., and P. J. Mason, 1990: Cloud-top entrainment instability through small-scale mixing and its parameterization. *J. Atmos. Sci.*, **47**, 1012–1030.
- Moeng, C.-H., 2000: Entrainment rate, cloud fraction, and liquid water path of PBL stratocumulus clouds. *J. Atmos. Sci.*, **57**, 3627–3643.
- , and U. Schumann, 1991: Composite structure of plumes in stratus-topped boundary layers. *J. Atmos. Sci.*, **48**, 2280–2291.
- Nicholls, S., 1989: The structure of radiatively driven convection in stratocumulus. *Quart. J. Roy. Meteor. Soc.*, **115**, 487–511.
- , and J. R. Leighton, 1986: An observational study of the structure of stratiform cloud sheets. Part I. Mean structure. *Quart. J. Roy. Meteor. Soc.*, **112**, 391–426.
- , and J. D. Turton, 1986: An observational study of the structure of stratiform cloud sheets. Part II. Entrainment. *Quart. J. Roy. Meteor. Soc.*, **112**, 461–480.
- Randall, D. A., 1980: Conditional instability of the first kind upside-down. *J. Atmos. Sci.*, **37**, 125–130.
- Rogers, D. P., and J. W. Telford, 1986: Metastable stratus tops. *Quart. J. Roy. Meteor. Soc.*, **112**, 481–500.
- Shy, S. S., and C. S. Bretherton, 1990: Laboratory experiments on the cloud-top entrainment instability. *J. Fluid Mech.*, **214**, 1–15.
- Siems, S. T., C. S. Bretherton, M. B. Baker, S. Shy, and R. T. Breidenthal, 1990: Buoyancy reversal and cloudtop entrainment instability. *Quart. J. Roy. Meteor. Soc.*, **116**, 705–739.
- Stevens, B., and Coauthors, 2003a: Dynamics and chemistry of marine stratocumulus—DYCOMS II. *Bull. Amer. Meteor. Soc.*, **84**, 579–593.
- , and Coauthors, 2003b: On entrainment rates in nocturnal marine stratocumulus. *Quart. J. Roy. Meteor. Soc.*, **129**, 3469–3493.
- Telford, J. W., and T. S. Keck, 1988: Atmospheric structure generated by entrainment into clouds. *Atmos. Res.*, **22**, 191–216.
- Vali, G., R. D. Kelly, J. French, S. Haimov, D. Leon, R. E. McIntosh, and A. Pazmany, 1998: Finescale structure and microphysics of coastal stratus. *J. Atmos. Sci.*, **55**, 3540–3564.
- VanZanten, M. C., and P. G. Duynkerke, 2002: Radiative and evaporative cooling in the entrainment zone of stratocumulus—The role of longwave radiative cooling above cloud top. *Bound.-Layer Meteor.*, **102**, 253–280.
- Wang, Q., and B. A. Albrecht, 1994: Observations of cloud-top entrainment in marine stratocumulus clouds. *J. Atmos. Sci.*, **51**, 1530–1547.
- , and D. H. Lenschow, 1995: An observational study of the role of penetrating cumulus in a marine stratocumulus-topped boundary layer. *J. Atmos. Sci.*, **52**, 2778–2787.